DOI: 10.6060/mhc256738s

The Smart Photosensitizer Chlorin e_6 (Fotoditazin®): the Role of Acid-Base Ionization

Vladimir B. Sheinin,[@] and Olga M. Kulikova

G.A. Krestov Institute of Solution Chemistry of the Russian Academy of Sciences, 153045 Ivanovo, Russia
[@]Corresponding author E-mail: vbs@isc-ras.ru

Dedicated to Corresponding Member of the Russian Academy of Sciences G.N. Vorozhtsov on the occasion of his 90th Anniversary

Photosensitizer chlorin e_6 meets almost all the basic requirements for an optimal photosensitizer formulated by scientists and experts. This work is devoted to the theoretical and experimental study of chlorin e_6 acid-base properties related directly to its interaction with transport proteins, lipid membrane and vesicle receptors along the entire path from the injection and entry into the bloodstream to reaching the target tumor and the specific key organelles. Generally, depending on the pH, the chlorin e_6 molecule can undergo stepwise acid-base ionization at three peripheral carboxyl groups and one intracyclic nitrogen atom of the chlorin platform, forming a series of amphiphilic ions. Protonation of chlorin platform is accompanied by a clear optical response in the absorption and fluorescence spectra, associated with photosensitizer phototoxicity under photodynamic therapy conditions, as well as its aggregation and lipophilicity. The results obtained were consistent and consolidated with the published data on acid-base ionization of the three peripheral carboxyl groups of chlorin e_6, and then were used to quantify the interfacial distribution coefficients between octanol-1 and phosphate-buffered saline. The study concluded that protonation of chlorin platform is likely the reason for the high selectivity of photosensitizer Fotoditazin® accumulation in tumor tissue.

Keywords: Chlorin e_6, PDT photosensitizers, Fotoditazin®, acid-base ionization, p*H*-dependent interfacial distribution coefficients.

«Умный» фотосенсибилизатор хлорин e_6: роль кислотно-основной ионизации

В. Б. Шейнин,[@] О. М. Куликова

Институт химии растворов им. Г.А.Крестова Российской академии наук, 153045 Иваново, Россия
[@]E-mail: vbs@isc-ras.ru

Фотосенсибилизатор Хлорин e_6 можно назвать даром природы для фотодинамической тераностики опухолей различной локализации. Он удовлетворяет практически всем основным требованиям, предъявляемым к оптимальному фотосенсибилизатору, основанным на фотофизических, биологических и химико-технологических критериях, которые были сформулированы учеными и специалистами в результате анализа большого объема экспериментальных и клинических материалов. Настоящая работа посвящена теоретическому и экспериментальному исследованию кислотно-основных свойств хлорина e_6, которые непосредственно связаны с его взаимодействием с транспортными белками, липидной мембраной и везикулами- рецепторами на протяжение всего пути от иньекции PS в кровоток до опухоли-мишени и ее органелл. В общем случае в зависимости от pH молекула хлорина e_6 может подвергаться пошаговой кислотно-основной ионизации по трем периферийным карбоксильным группам и по одному внутрициклическому атому азота хлориновой платформы, образуя череду амфифильных ионов. Протонирование хлориновой платфлормы, сопровождается четким оптическим откликом и оказывает непосредственное влияние на спектры поглощения и флуоресценции этого PS, которые связанные с его фототоксичностью в условиях ФДТ, а также на его агрегационное состояние и липофильность. Полученные результаты были согласованы и консолидированы с литературными данными по кислотно-основной ионизации трех периферийных карбоксильных групп хлорина e_6, а затем были использо-

ваны для количественной интерпретации коэффициентов его межфазного распределения между октанолом-1 и PBS. Сделан вывод, что протонирование хлориновой платформы является причиной высокой селективности накопления фотосенсибилизатора Fotoditazin® в тканях злокачественных новообразований.

Ключевые слова: Хлорин e_6, фотосенсибилизаторы ФДТ, Фотодитазин®, кислотно-основная ионизация, p*H*-зависимые коэффициенты межфазного распределения.

Introduction

The photosensitizer chlorin e_6 can be described as a gift of Nature provided for the using in photodynamic diagnosis and therapy of different located tumors.[1–7] It meets almost all the basic requirements for an optimal photosensitizer (PS) based on photophysical, biological and chemical-engineering criteria that were formulated by scientists and experts as a result of the analysis of a large amount of experimental and clinical data.

1. Strong absorption in the spectral range of the "therapeutic window", where biological tissues have the highest transmission ($\varepsilon_{655nm} = 2.5 \cdot 10^4$, saline solution, p*H* 7.7, data obtained from our own experiments).
2. The fluorescence quantum yield which is sufficient for fluorescent diagnosis allowing to control the accumulation and elimination of PS from the tissues (Φ_F = 0.16–0.22 aqueous media,[8,9] Φ_F =0.18/p*H* 7.4 PBS, Φ_F =0.24 chlorin e_6–polyvinylpyrrolidone/p*H* 7.4,[10] Φ_F =0.11/distilled water,[11] Φ_F =0.18/p*H* 7.2 Tris-HCl[11]).
3. High quantum yield of singlet oxygen generation (Φ_Δ = 0.67± 0.07/p*H* 8.5, 0.60± 0.06/p*H* 7.4 in PBS and 0.50± 0.05/p*H* 6.3 in Tris-HCl[12,13]).
4. High solubility in water or intravenous fluids and blood substitutes (the formulation Fotoditazin® is a dimeglumine salt of chlorin e_6, which increases the solubility of organic acids, but does not affect the therapeutic effect of drugs)
5. High selectivity of accumulation in malignant neoplasms (the tropism of Fotoditazin® reaches 20 after 1.5-2.5 h from the injection moment[14]).
6. Rapid photosensitizer elimination from skin and epithelial tissue ($T_{1/2}$ = 12 for Fotoditazin® [14]).
7. Low dark and light toxicity in therapeutic doses (Fotoditazin® exhibited the lack of dark toxicity in therapeutic doses[14]).
8. Storage stability (the shelf life of Fotoditazin® is 1 year at a temperature as high as 10 °C[14]).
9. Availability of manufacturing or synthesis, uniform chemical composition.

The key feature of PS chlorin e_6 is its inexhaustible natural raw material base. The main source of pure chlorin e_6 is the blue-green algae *Spirulina platensis*, which is cultivated on a large scale as a high-demand superfood and detox product. In 2025, the volume of global sales of *Spirulina platensis* powder will amount to about 600 million dollars, and is expected to increase more than one and a half by 2032.[15]

This work is devoted to the theoretical and experimental study of the acid-base properties of chlorin e_6, related directly to its interaction with transport proteins, lipid membrane and vesicle receptors along the entire path from the injection and entry into the bloodstream to reaching the target tumor and the specific key organelles like nucleus, mitochondria, lysosomes, and endoplasmic reticulum.[16–20] The p*H* of the interstitial fluid in tumors is known to be lower than in normal tissues.[21–23] There is a fairly significant variation in p*H* inside the tumor, when this value can reach 5.55.[22] The p*H* gradient is a determining factor in the selective uptake of carboxyl-containing PS by cancer tumors.[16,24–26] In the acidic tumor microenvironment, the affinity of chlorin e_6 to the transport proteins decreases then the affinity to the lipid membrane, penetration speed and depth increased.[19]

Experimental

Chemicals

All commercial reagents (Sigma-Aldrich) were used as received without further purification. Phosphate-buffered saline solution p*H* 7.4 (PBS) was prepared using appropriate amounts of Na_2HPO_4 and KH_2PO_4 in double-distilled water. Deuteroporphyrin IX dimethyl ester was synthesized according to[27]. The medicine Fotoditazin® (“VETA-GRAND”) was used as a source of chlorin e_6 dimeglumine salt. Triammonium salt of chlorin e_6 (triammonium salt of 18-carboxy-20-(carboxymethyl)-8-ethenyl-13-ethyl-2,3-dihydro-3,7,12,17-tetramethyl-21H,23H-porphin-2-propionic acid) was synthesized and purified according to modified procedure presented in [28]. Dimeglumine salt of chlorin e_6 (Fotoditazin®) was treated carefully with 17.5% hydrochloric acid solution at a temperature of 10 °C until complete precipitation of chlorin e_6. The chlorin e_6 precipitate was separated from the supernatant by centrifugation and washed with distilled water. Wet precipitate of chlorin e_6 was treated with a minimal amount of a weak aqueous ammonia solution at a temperature of 10 °C until the chlorin e_6 was completely dissolved and a p*H* of 9.5 was reached. The resulting triammonium salt of chlorin e_6 was used to prepare working solutions.

Instruments

The absorbance and fluorescence spectra were recorded synchronous at 25 °C and 36.6 °C in 1×1 cm optical quartz cell using a fluorescence spectrophotometer (AvantesAvaSpec 2048-2) equipped with a qpod© (Temperature-Controlled Sample Compartment for Fiber Optic Spectroscopy). The monochromatic LEDs 5P4FCA, 3-4mW, λ_{max}=401 nm, VL400-5-15, 8.1-11.5mW, λ_{max}=402 nm, (Roitner Lasertechnik Gmbh., Germany) were used as light sources for fluorescence study. Micropipette with the scale value is $5.5 \cdot 10^{-6}$ mL was used for titration experiment. The pH values were measured using InLab Micro pH electrode (Mettler-Toledo Inc.). The protonation constants were calculated using SigmaPlot® (Systat Software Inc. (SSI)) software.

All calculations have been performed at the B3LYP 6-31++G(d,p) level of DFT using the Gaussian software package.[29] No imaginary frequencies were obtained after vibrational analysis of the optimized structures

Results and Discussion

The structure and acid-base properties of chlorin e_6

Chlorin e_6 is a unique molecular structure with a p*H* dependent charge and lipophilicity. It consists of a bulky alkyl-substituted chlorin platform H_2C (lipophilic part) and three close-packed residues of methanoic, ethanoic and propanoic acids (hydrophilic part) at the molecule periphery (Figure 1).

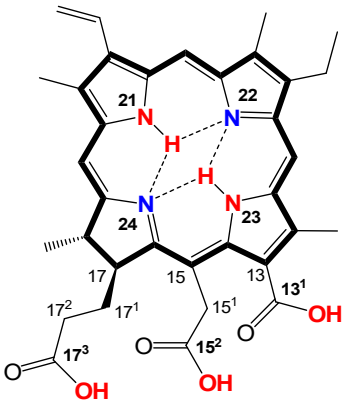

Figure 1. The molecular structure of chlorin e_6 (H_2Ce_6). The chlorin platform H_2C is indicated by thick line. Acidic and basic centers are shown in red and blue, respectively. The dotted line represents four bifurcated intramolecular hydrogen bonds (IMHB). Some atoms numbering will be used hereafter.

Generally, depending on the p*H* of the medium, the chlorin e_6 molecule can undergo acid-base ionization by three peripheral carboxyl groups and four intracyclic nitrogen atoms as a part of two pyrrole (>NH) and two pyrrolenine (≥N) groups, forming a series of amphiphilic ions. Despite the large number of publications deals with chlorin e_6 investigation, its acid-base ionization is still poorly known. Here we investigated the acid-base ionization of chlorine_6 in saline solution, which is accompanied by a clear optical response in the absorption and fluorescence spectra, associated with PS phototoxicity under PDT conditions, as well as its aggregation and lipophilicity. The results obtained were consistent and consolidated with the published data on the acid-base ionization of the three peripheral carboxyl groups of chlorin e_6, and then were used to quantify the interfacial distribution coefficients between octanol-1 and PBS.

Acid-base ionization of chlorin e_6 from first principles

The general order of acid-base ionization of seven functional groups of chlorin e_6 can be determined in terms of proton affinity PA ($-\Delta_g H_b^0$) based on the theoretical values of stepwise enthalpies of protonation $\Delta_g H_{bi}^0$ in the gas phase, which correspond to $\lg K_{bi}$ in solution.[30,31] Hereinafter, for the simplicity, the abbreviation H_2C will be used to denote a chlorin platform with any substituent system and to describe the protolysis of intracyclic ≥N and >NH groups of H_2C, neglecting the peripheral substituents. In the first step, a DFT study of the features of the chlorin molecule H_2Chl (unsubstituted chlorin platform H_2C) protolysis was carried out. Unlike the porphine H_2Por (unsubstituted porphine platform H_2P), chlorin has one (of two) hydrogenated "semi-isolated" 17,18-bond (Scheme 1), which affected the physicochemical and acid-base properties of chlorins significantly. Two tautomers 21,23-H_2Chl and 22,24-H_2Chl are possible for the unsymmetrical H_2Chl molecule, differing in the position of the NH groups relative to the hydrogenated bond position.

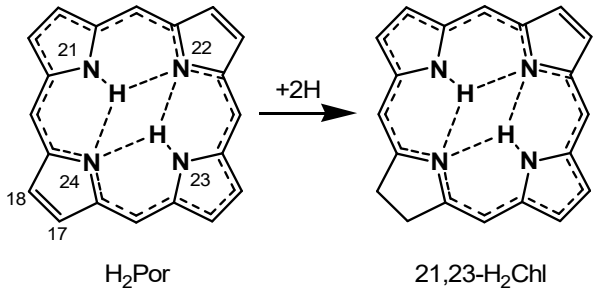

Scheme 1. The structure of unsubstituted porphyrin and chlorin platform. The figure presents the semi-insulated double bonds and the main conjugated contour which highlighted with a solid plus dashed lines.

DFT calculations of the standard enthalpy values of these tautomers formation $\Delta_g H_f^o$ have shown that 21,22-H_2Chl tautomer is 6.64 kcal/mol more stable than an alternative 22,24-H_2Chl tautomer (Table 1). Thus, the 21,23-H_2Chl tautomer was used as a base structure for further calculation of the molecular parameters of chlorin e_6 and its acid-base forms. As well as H_2Por, the 21,23-H_2Chl molecule has a flat aromatic platform with four intramolecular bifurcate hydrogen bonds (IMHB) (Figure S1), which are formed as a result of intramolecular tightness.[32,33] These IMHB stabilized the planar structure of the tetrapyrrole macrocycle and blocked intramolecular acid-base centers from non-covalent interactions with solution components. The protolysis of the intramolecular acidic NH or basic N groups of 21,23-H_2Chl, also as in the case of H_2Por, results in the formation of four ionic forms (Equation (1)):

$$C^{2-} \xleftarrow{-H^+} HC^- \xleftarrow{-H^+} H_2C \xrightarrow{+H^+} H_3C^+ \xrightarrow{+H^+} H_4C^{2+} \quad (1)$$

For H_3Chl^+, two tautomers are possible: 21,22,23-H_3Chl^+ and 21,23,24-H_3Chl^+ ,differing in the excess proton position (Scheme 2).

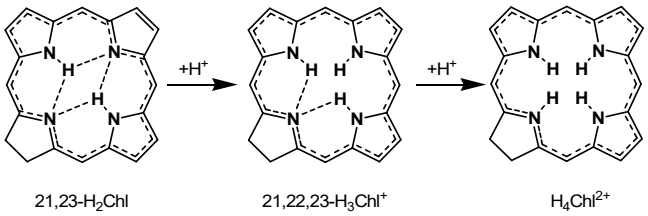

Scheme 2. The most stable tautomers of chlorin and its protonated forms.

Table 1. DFT-calculated (DFT/B3LYP/6-31^{++}G(d,p)) parameters of H_2Por, Por^{2-}, H_2Chl and Chl^{2-} protonation (Equations (2), (3)), aqua- and hydrogensulfate complexes $H_4Por^{2+}(G)_2$, $H_4Chl^{2+}(G)_2$ formation (Equation (4))

Compound	$\Delta_gH_{b1}^o$ (kcal/mol)	$\Delta_gH_{b2}^o$ (kcal/mol)	$\Delta_gH_{2G}^o$ (kcal/mol)	L (Å)	angle HB (degree)	ΣΔQ (ē)	$\Delta_gH_{2G}^o$ (kcal/mol)	L (Å)	angle HB (degree)	ΣΔQ (ē)
				G=H_2O				G=HSO_4^-		
H_2Por	-238.77	-159.79	-29.65	4.46	169.30	-0.35	-253.06	3.72	173.81	-0.89
Por^{2-}	-435,72	-348,50								
H_2Chl	-241.97	-153.42	-29.36	4.41	168.40	-0.36	-254.90	3.66	174.30	-0.90
Chl^{2-}	-436,46	-350,42								

$\Delta_gH_{bi}^o$ –stepwise enthalpies of protonation
$\Delta_gH_{2G}^o$ – enthalpies of complexes formation
L - distance between the contact oxygen atoms of the "guests"(G).
ΣΔQ - total transferred charge from two "guests" to a diprotonated macrocycle.

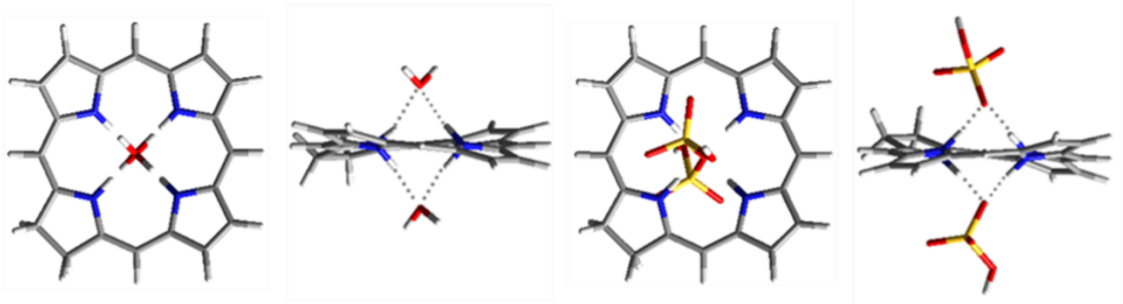

$[H_4Chl^{2+}](H_2O_2)_2$ **$[H_4Chl^{2+}](HSO_4^-)_2$**

Figure 2. DFT-calculated geometry of H_4Chl^{2+} "double roost" type complexes. The H_4C^{2+} platform exist in 1,3-alternate configuration.

The 21,22,23-H_3Chl^+ which formed as a result of protonation of nitrogen atom 22 is more stable. As in the case of H_3Por^+, the two bifurcated intramolecular HB blocked the acid-base centers of 21,22,23-H_3Chl^+ from non-covalent interactions with solution components. Hydrogenation of the 17,18-bond in H_2Por increases the PA of 21,23-H_2Chl by 3.2 kcal/mol, and decreases the PA of 21,22,23-H_3Chl^+ by 6.37 kcal/mol which implies an increase in the chlorins basicity at the first step of protonation in solutions and increase in the difference between the stepwise protonation constants compared to structurally similar porphyrins.

The accession of a second proton completely disrupts the IMHB. Dication H_4Chl^{2+}, as well as H_4Por^{2+}, has the 1,3-alternate structure, which is formed as a result of the Van der Waals and electrostatic repulsion of hydrogen atoms of four intracyclic NH groups (Figure S2). The positively charged 1,3-alternate exibits the receptor properties and exists in aqueous solutions only as a homogeneous or mixed complexes $[H_4P^{2+}](H_2O)_2$, $[H_4P^{2+}](An^-)_2$ and $[H_4P^{2+}](H_2O)(An^-)$, respectively.[33–41] According to DFT calculations, the H_4C^{2+} is also capable of forming "double roost" type complexes with water and anions, which stability is compared with corresponding porphyrin complexes (Figure 2, Table1).

$$H_2C + H^+ \xrightarrow{\Delta_gH_{b1}^0} H_3C^+ \quad (2)$$

$$H_3C^+ + H^+ \xrightarrow{\Delta_gH_{b2}^0} H_4C^{2+} \quad (3)$$

$$H_4C^{2+} + 2G \xrightarrow{\Delta_gH_{2G}^0} [H_4C^{2+}](G_2);\ G = H_2O \text{ or } HSO_4^- \quad (4)$$

Table 1 shows that the basic properties of H_2Chl are much more pronounced than the acidic ones, which coincides with the acid-base ionization of H_2Por in solution. Within the unified pH scale[42] the known experimental values of protonation and deprotonation constants lgK_{b1} and pK_{a1} for H_2Por are 3.59 and 22.35, respectively.[35] In this case, the value of first protonation constant of H_2Por lies within the boundaries of the aqueous pH scale, while the value of first deprotonation constant is well beyond its upper boundary, and therefore we do not consider the deprotonation of chlorin e_6 in this work.[39]

At the next step, the DFT geometry was optimized and the enthalpies of formation $\Delta_gH_f^o$ of the chlorin e_6 trianion ($H_2Ce_6^{0/-3}$) and its all possible protonated forms with the general formula $H_nCe_6^{p/m}$, linked by Equation (5), were calculated.

$$p + m = n - 5, \quad (5)$$

where n is the total amount of mobile hydrogens, p – the charge of the chlorin platform, m- the total charge of carboxylate groups.

Based on the Δ_gH_{fo} values, the order of trianion $H_2Ce_6^{0/3-}$ stepwise protonation and stepwise proton affinity PA_i ($-\Delta_gH_{bi}^o$) of its most stable protonated forms were determined (Scheme 3). The calculation showed that 13^1, 15^2, and 17^3 carboxylate groups of the chlorin e_6 hydrophilic part should be protonated first one after another to

form the electroneutral structure $H_5Ce_6^{0/0}$, and then 23 and 24 pyrrolenine nitrogen atoms of the chlorin platform protonated to form the final dication $H_7Ce_6^{2+/0}$.

The acid-base ionization of chlorin e_6 in aqueous solutions: carboxyl groups

The study of the acid-base ionization of the carboxyl groups of chlorin e_6 presents some difficulties due to the lack of H_2C optical response, as well as due to the tendency of chlorin e_6 molecules with a large hydrophobic mass (199.9 u per carboxyl group) to association and aggregation in aqueous media, which increase with decreasing the total negative charge and increasing the ionic strength.[16] M. Vermathen and co-workers measured the lgK_{b1}, lgK_{b2} and lgK_{b3} of chlorin e_6 3^1, 5^1 and 7^1 carboxyl groups by ^{13}C NMR spectroscopy in H_2D, with values of 8.3 ± 0.1, 7.9 ± 0.1 and 7.9 ± 0.1 at 25°C, respectively.[43]

The acid-base ionization of chlorin e_6 in aqueous solutions: chlorin platform

Hydrogenation of the 17,18-bond of the porphyrin platform is the cause of the red shift and sharp increase in the intensity of the long-wavelength absorption band Q_1 (12.5-fold, Figure 3), as well as the fluorescence enhancement in the 'therapeutic window' region, which are important for photodynamic theranostics.

In the p*H* range from 8 to 6, a characteristic optical response of H_2C is observed for chlorin e_6 aqueous solution, accompanied by a blue shift and a partial decrease in the intensity of the Q_1 absorption band, and identical changes in the fluorescence spectra.[16,20] Whereas these spectral changes are similar with the optical response of H_2C single protonation in non-aqueous solutions (Table 2)[45,46] this response is traditionally attributed to the aggregation of electroneutral molecules $H_5Ce_6^{0/0}$[16] that are formed as a result of the exhaustive protonation of the three carboxylate groups in aqueous media, ignoring alternative protonation of H_2C. At the same time, it is postulated that protonation of carboxylate groups and the degree of chlorin e_6 aggregation are the main factors determining its membrane adsorption, rate and depth of molecule diffusion through phospholipid bilayers,[16–20,43,47–49] as well as an increase in chlorin e_6 distribution constants between nonpolar octanol-1 and aqueous medium,[10,16,50–52] while protonation of one intracyclic nitrogen prevents incorporation of the molecule into the hydrophobic layer of the phospholipid membrane.

The optical spectra of chlorin e_6 protonated forms H_2C, H_3C^+ and H_4C^{2+} were recorded in the binary methanol-H_2SO_4 medium (Figure 4) for subsequent identification of these forms in saline solution.

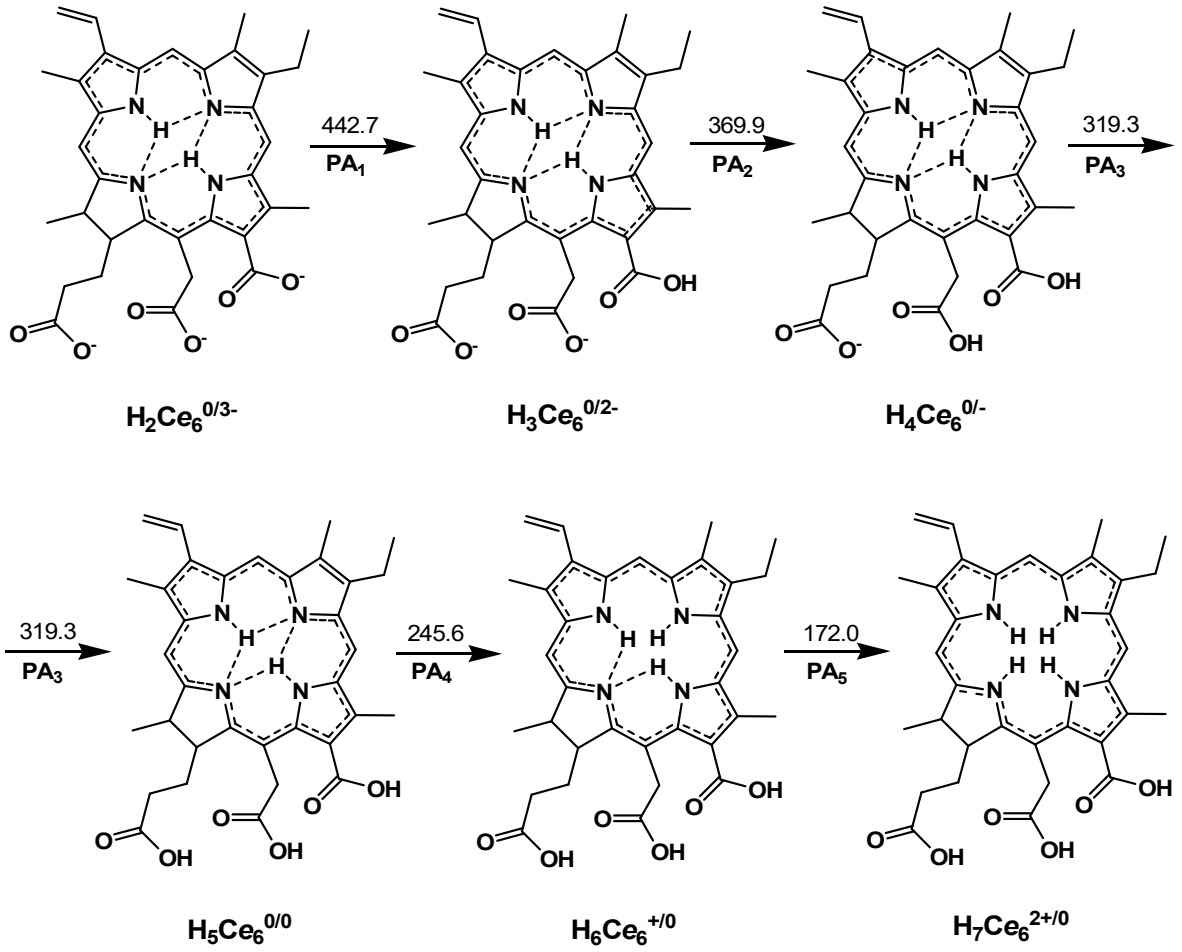

Scheme 3. The order of stepwise protonation of chlorine e_6 trianion $H_2Ce_6^{0/3-}$ based on PA_i values (kcal/mol).

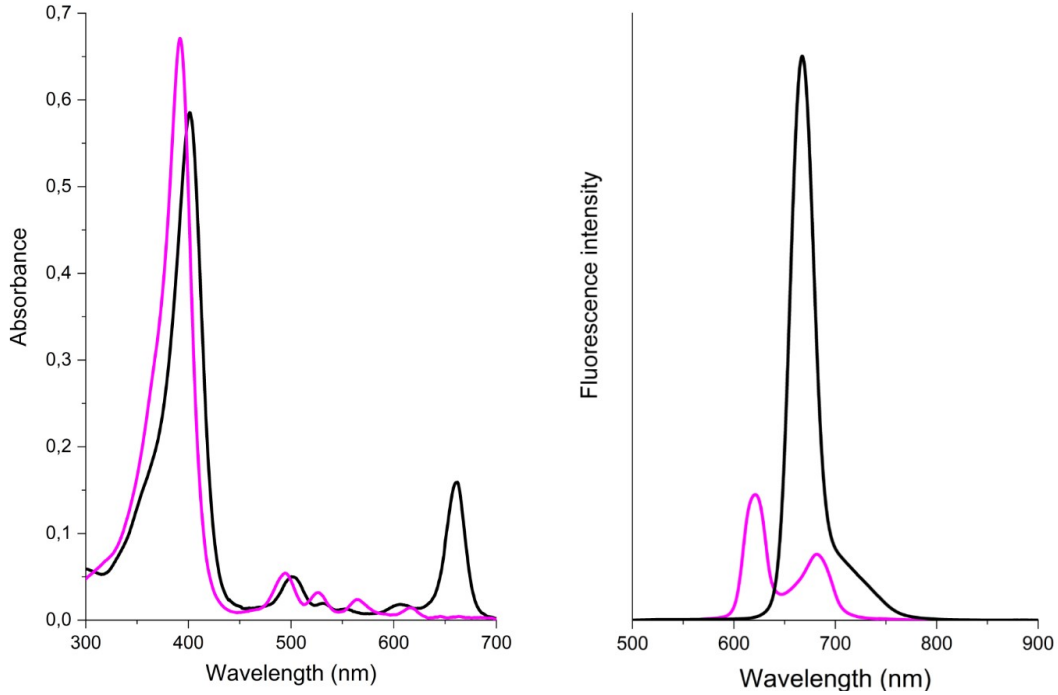

Figure 3. Optical spectra of methanol solutions (c=3.96·10^{-6}M) of deuteroporphyrin IX dimethyl ester (ε_{617} =3490 [44]) - marengo line and chlorine_6 (ε_{662} = 43700 [45]) - black line at 25 °C . Fluorescence excitation at 401nm.

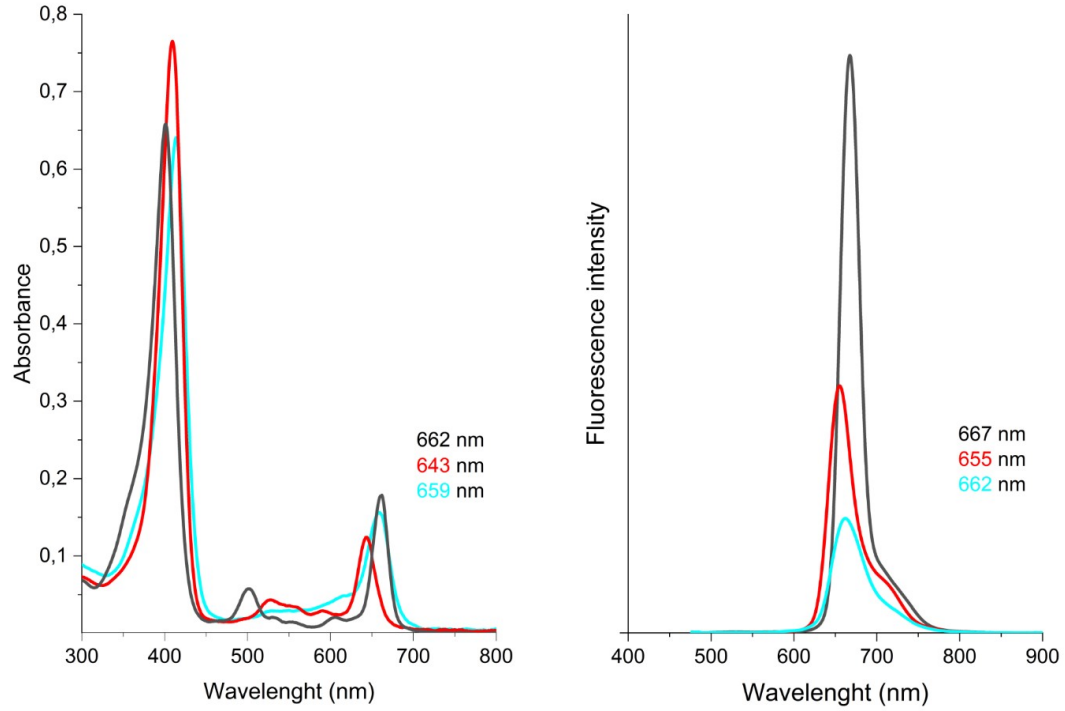

Figure 4. Optical spectra of chlorin e_6 solutions (c=4.09·10^{-6}M): H_2C (black), H_3C^+ (red), and H_4C^{2+} (blue) in methanol-H_2SO_4 binary medium at 25 °C. Fluorescence excitation at 401 nm.

Methanol is a convenient boundary solvent between aqueous and organic media. It has sufficient solvent capacity towards natural tetrapyrroles to provide their aggregation stability. In addition, methanol has a sufficiently high dielectric constant (ε=32.63 at 25 °C), which is necessary for ionic processes to occur. The optical spectra of chlorin e_6 methanol solutions with H_2C, H_3C^+ and H_4C^{2+} are identical to the spectra of other natural chlorines and lack signs of intermolecular association.

Protonation of chlorin platform of Fotoditazin® in saline solution at 36.6 °C

Further in our work we used highly water-soluble dimeglumine salt of chlorin e_6 (**H_2C**e_6 d.m.s.) which is used as PDT photosensitizer Fotoditazin® (Figure 5) with a drug strength of 10 mg/ml.

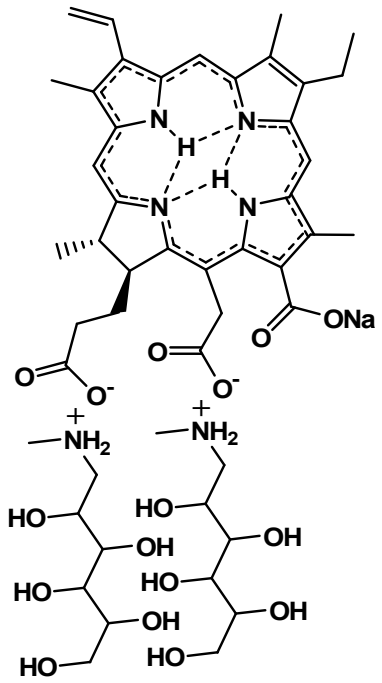

Figure 5. Dimeglumine salt of chlorin e_6 (Fotoditazin®).

Fotoditazin® is a successful example of the practical use of meglumine to enhance the solubility and aggregation stability of chlorin e_6. Meglumine increases the solubility of organic acids, but does not affect the therapeutic effect of drugs. In an aqueous solution, the dimeglumine salt decomposes to form free chlorin e_6. The initial optical spectra of Fotoditazin® in saline solution are completely identical to the spectra of triammonium salt of chlorin e_6 (H_2Ce_6t.a.s.) in methanol (Table 2, Figure S3), indicating the absence of intermolecular association, at least at concentrations up to $6.00 \cdot 10^{-6}$ M (Figure S4). During the acid titration of dimeglumine salt of chlorin e_6 in saline solution, transformation of chlorin e_6 optical spectra corresponds only the first stage of H_2C protonation at the 24 nitrogen atom is observed (Figure 6, Figure 4), while the second protonation stage is expected in a more acidic region. Two clearly defined areas of the spectropotentiometric titration curves corresponding to two different equilibrium protolytic processes can be distinguished (Figure 6).

In the pH range of 8.5–5.4, the optical spectra of chlorin e_6 platform H_2C are transformed directly into the spectra of H_3C^+ with Q_1 maxima of the absorption and fluorescence bands at 655 nm and 664 nm, respectively. In synchronous optical spectra, clear isosbestic and isoemission points (Figure S5) are observed, indicating equilibrium only between these two optical centers, which we see to be insensitive to ionization of the peripheral carboxylate groups, as well as to the presence of meglumine.

Thus, the first section of the H_2Ce_6 d.m.s. titration curve corresponds to the protonation of the 24th nitrogen atom of H_2C. In the second region, in the range of p*H* 5.4-3.0, a monotone decreasing in the intensity of the H_3C^+ absorption spectrum is observed, with a small blue shift of 3 nm, but the fluorescence decreases insignificantly. In this case, the partial solution bleaching is caused by the partial formation of a precipitate, which is in protolytic equilibrium with the solution. The solid phase is concentrated on the Teflon magnetic stirrer surface and does not create the effect of suspension light scattering. The equilibrium spectrum of chlorin e_6 with protonated H_3C^+ remains unchanged at p*H* 3 overnight, indicating its aggregation stability. Thus, the second stage of the titration curve corresponds to the interfacial protolytic equilibrium between the solution of chlorin e_6 with H_3C^+ and the precipitate of unknown composition. The likely cause of precipitation is the formation of J-aggregates of unknown composition (see chapter *Acid-base ionization of chlorin e_6 from first principles*), which study goes beyond the scope of this report.

Table 2. Optical spectra parameters of chlorin e_6 and its protonated forms in different media.

Compound	Medium	Soret Band, (nm)			Q_1 Band, (nm)		
		H_2C	**H_3C^+** (red shift)	**H_4C^{++}** (red shift)	**H_2C**	**H_3C^+** (blue shift)	**H_4C^{++}** (red shift)
Chlorin e_6 t.m.e.[45]	CH_3OH-HCl	398	409	420	662	644	662
Chlorin e_6 t.m.e.[45]	CH_3COOH	-	408	422	-	644	663
Chlorin e_6*	CH_3OH-CF_3COOH	402	409	-	660	642	-
Chlorin e_6*	CH_3OH-H_2SO_4	402	411	415	663	647	657
Chlorin e_6 d.m.s.*	CH_3OH-H_2SO_4	401	410	414	662	643	659
Chlorin e_6[16]	H_2O-PBS	401	406	-	654	639	-
Chlorin e_6 d.m.s *	H_2O-H_2SO_4	402	405		655	642	

t.m.e. – trimethyl ester, d.m.s. –dimeglumine salt (Fotoditazin®)
*) – this research data.

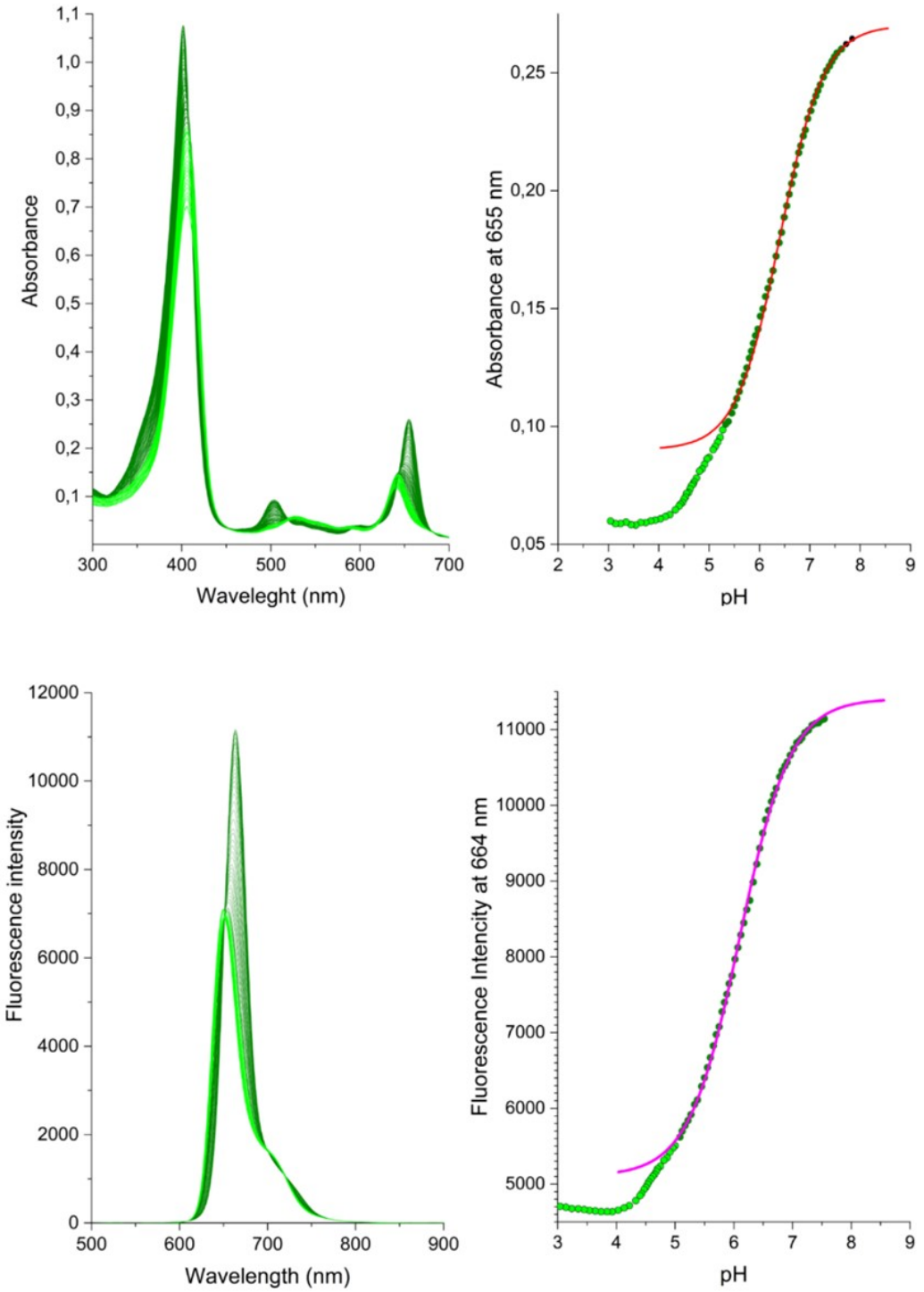

Figure 6. The results of spectropotentiometric titration of H_2Ce_6 d.m.s. with sulfuric acid in saline solution at 36.6 °C. First protonation step of H_2C is shown indark-green color, and the second stage is shown in green. The red line shows the titration curves obtained by fitting the parameters in Equation (6).

The first part of absorption and fluorescence titration curves was approximated by Equation (6) for the first step of H_2C protonation (Equation (7)).

$$Y_{\lambda} = \frac{Y_{0(H_2C)} + Y_{0(H_3C^+)} \times K_{b4} \times 10^{-pH}}{1 + K_{b4} \times 10^{-pH}}, \qquad (6)$$

where Y_{λ} – current value of absorbance (A) or fluorescence (F) on analytic wavelength λ, $Y_{0(i)}$ – absorbance or fluorescence of i-form solution with a concentration equal to the analytical concentration of H_2Ce_6 d.m.s

$$H_2C + H^+ \underset{}{\overset{K_{b4}}{\rightleftarrows}} H_3C^+ \qquad (7)$$

The calculation performed by fitting the parameters K_{b4} and $Y_{o(H3C+)}$ in Equation (6) showed that the first region of the titration curve of dimeglumine salt of chlorin e_6

corresponds exactly to the one-proton Equilibrium (7) with constants $^{A}K_{b4}$=6.40±0.03 and $^{F}K_{b4}$=6.01±0.03. The difference between the absorption $^{A}K_{b4}$ and fluorescence $^{F}K_{b4}$ protonation constants exceeds the error of determination, is due to the different basicity of H_2C in the ground and excited states.

The effect of meglumine

To evaluate the contribution of meglumine to the acid-base properties and aggregation p*H* stability of Fotoditazin®, a comparative study of chlorin e_6 triam-monium salt (H_2Ce_6 t.a.s.) in saline solution were carried out. The first difference is the blue and red broadening of the absorption bands of H_2Ce_6 t.a.s. in the initial saline solution with a p*H* 8.5 compared to the spectra of H_2Ce_6 d.m.s. (Figure 7), which indicates the presence of H-aggregates (blue shift) and J-aggregates (red shift), respectively. These chlorin e_6 aggregates may have the same structure as proposed by L. M. Scolaro and co-workers for protoporphyrin IX.[53] The chlorin e_6 aggregates exhibit no fluorescence, allowing the monomers to be observed independently.

Monomer and aggregates of chlorin e_6 interact with the acid differently. The monomer is protonated in two steps similar to H_2Ce_6 d.m.s. (Figure S6). The first section of the titration curve is characterized by clear isosbestic and isoemissive points in the absorption and fluorescence spectra corresponds entirely to the protonation of the intracyclic nitrogen atom of the chlorin platform with $^{A}K_{b4}$ = 6.40 ± 0.03 and $^{F}K_{b4}$ = 6.10 ± 0.03, coinciding with the values for chlorin e_6 dimeglumine salt. Protonation of the chlorin e_6 monomer results in the formation of a mixture of chlorin e_6 with monoprotonated H_3C^+ and the initial non-fluorescent aggregates with absorption bands at 642 and 669.4 nm, respectively. The fluorescence maximum at 658.8 nm corresponds to the Q_1 absorption band of chlorin e_6 with H_3C^+, while its aggregates exhibit no fluorescence. With further acidification of this mixture, a p*H*-dependent equilibrium precipitate formation occurs. At this stage, there are no isosbestic and isoemissive points in the absorption and fluorescence spectra. Most of the initial chlorin e_6 aggregates pass directly into the precipitate, but a small amount of them are first broken down to monomers (the finish part of the fluorescence titration curve). Thus, meglumine has no appreciable effect on the protonation constants of the hydrophilic and hydrophobic portions of chlorin e_6 in aqueous solution. For this reason, only the H_2Ce_6 will be used instead of the H_2Ce_6 d.m.s. and H_2Ce_6 t.a.s abbreviation for simplicity.

Consolidated acid-base ionization constants of carboxyl groups and chlorin platform of chlorin e_6 in saline solution at 36.6 °C

After measuring the protonation constant of H_2C of chlorin e_6, we performed a procedure to consolidate K_{b4} with the protonation constants of the three carboxyl groups K_{b1}, K_{b2} and K_{b3} measured by ^{1}H NMR in H_2D.[54]

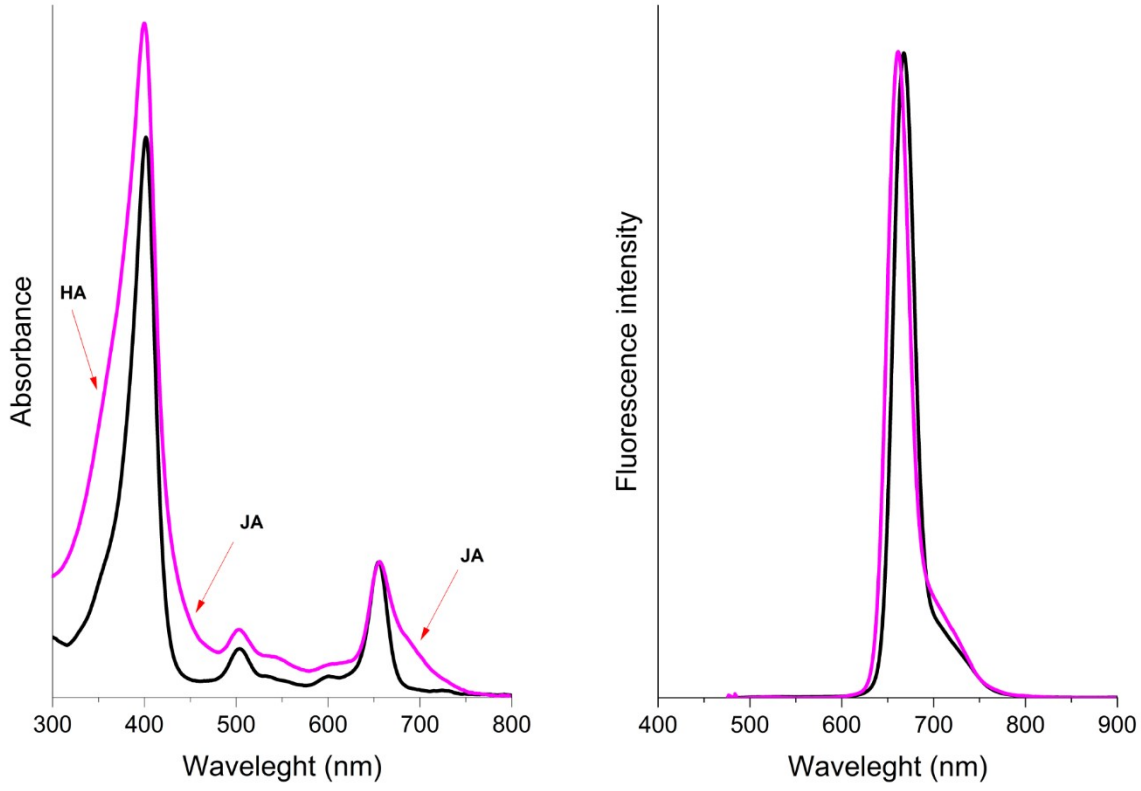

Figure 7. The optical spectra of H_2Ce_6 d.m.s (black) and H_2Ce_6 t.a.s.(marengo) in saline solution at 36,6 °C and pH 8.5, aligned to Q_1 bands and fluorescence intensity, respectively. Fluorescence excitation at 401nm. The arrows indicate the presence of H-aggregates (HA) and J-aggregates (JA).

To do this, we adjusted for the effect of deuterated solvent (Equation (8)) and estimated the correlation of experimental lgK_{bi} values of protolytic Equilibria (9)–(13) with PA_i for three carboxylate groups and a chlorin platform (Figure 8).

$$lgK_{bi}(H_2O) = lgK_{bi}(D_2O) - 0.48 \quad (8)$$

$$H_2Ce_6^{0/3-} + H^+ \underset{}{\overset{K_{b1}}{\rightleftharpoons}} H_3Ce_6^{0/2-} \quad (9)$$

$$H_3Ce_6^{0/2-} + H^+ \underset{}{\overset{K_{b2}}{\rightleftharpoons}} H_4Ce_6^{0/-} \quad (10)$$

$$H_4Ce_6^{0/-} + H^+ \underset{}{\overset{K_{b3}}{\rightleftharpoons}} H_5Ce_6^{0/0} \quad (11)$$

$$H_5Ce_6^{0/0} + H^+ \underset{}{\overset{K_{b4}}{\rightleftharpoons}} H_6Ce_6^{+/0} \quad (12)$$

$$H_6Ce_6^{+/0} + H^+ \underset{}{\overset{K_{b5}}{\rightleftharpoons}} H_7Ce_6^{2+/0} \quad (13)$$

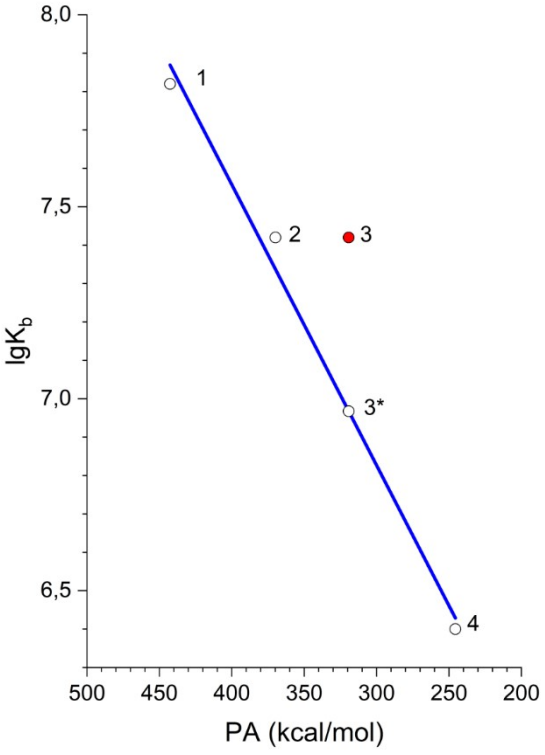

Figure 8. Correlation between the protonation constants lgK_{bi} of chlorin e_6 and the corresponding PA_i values: 1 – lgK_{b1}/PA_1, 2 – lgK_{b2}/PA_2, 3 – $lgK_{b3}//PA_3$, 3* – $lgK_{b3}^*//PA_3$, 4 – lgK_{b4}/PA_4.

The lgK_{b3} value of the carboxylate group 17[3] drops out of the correlation relationship, which has an unexpectedly large value coinciding with lgK_{b2} for 15[2], while a linear correlation with a coefficient of 0.995 for the three pairs of lgK_{b1}/PA_1, lgK_{b2}/PA_2 and lgK_{b4}/PA_4 values was obtained. The new refined value of lgK_{b3}^* determined from this dependence is 6.97. Thus, we see that the values of protonation constants of carboxylate groups in water can be used to describe the protonation equilibria of the hydrophilic part of chlorine e_6 in saline solution. The values of lgK_{b1}, lgK_{b2}, lgK_{b3}^* and lgK_{b4} were used to plot the p*H*-dependent concentration distribution of equilibrium forms of $H_nCe_6^{p/m}$ in saline solution at 36 °C (Figure 9). These dependencies are presented analytically in the Supporting materials (Equations S1-S5).

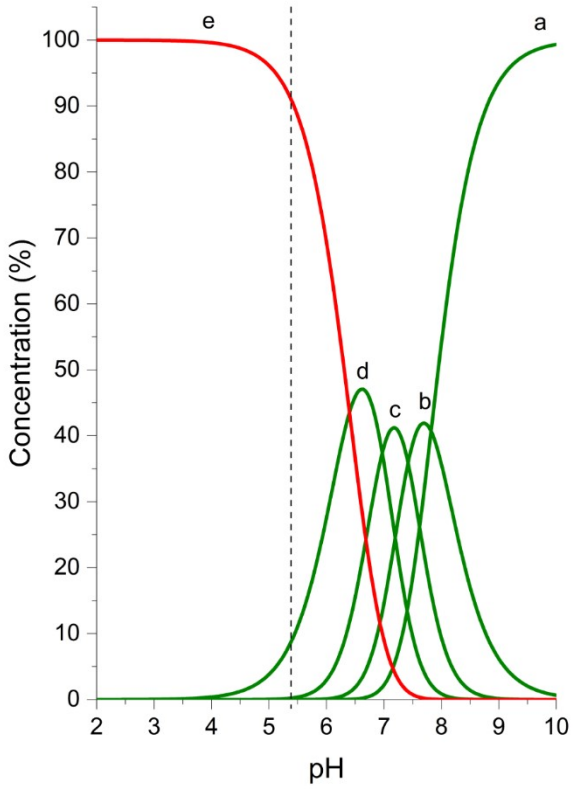

Figure 9. The p*H*-dependent distribution of equilibrium concentrations of the $H_nCe_6^{p/m}$ ionic forms in saline solution at 36.6 °C: a – $H_2Ce_6^{0/-3}$, b – $H_3Ce_6^{0/2-}$, c – $H_4Ce_6^{0/-}$, d – $H_5Ce_6^{0/0}$ (green lines), e – $H_7Ce_6^{+/0}$(red line), plotted based on lgK_{b1}, lgK_{b2}, lgK_{b3}^*, lgK_{b4}. The dashed line marked the boundary of sedimentation.

The protonation energy decreases dramatically as a result of solvation of the reagents in going from the gas phase (PA) to the solution (lgK_b)[30,31,55]. The medium effect leads to a significant convergence of the stepwise K_{bi} values in the saline solution, resulting in the mixing of Equilibria (9)-(13), as shown in Figure 9. Due to the close values of the step constants, all ionic forms of chlorin e_6 related by the system of dynamic Equilibria (9)-(13), are present in the physiologic pH range 5-8, which ultimately allows chlorin e_6 to adjust to a substrate of any polarity.

The effect of pH on the chlorin e_6 interfacial distribution between octanol-1 and PBS

When octanol-1 is added to the chlorin e_6 phosphate buffer solution, an interphase equilibrium is established (Scheme 4), as a result part of the chlorin e_6 passes into nonpolar octanol-1 (ε =10.3) exclusively in the electroneutral form $H_6Ce_6^{0/0}$.

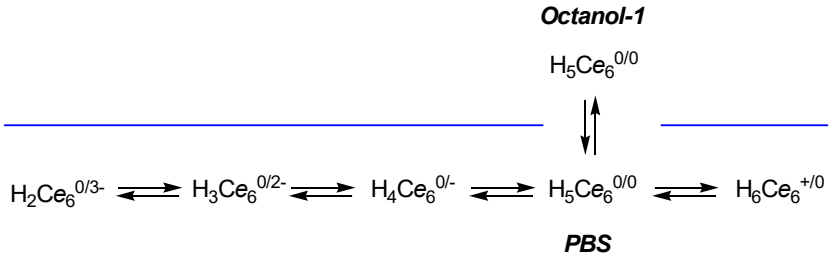

Scheme 4. The proposed scheme of equilibria between different forms of $H_nCe_6^{p/m}$ in a two-phase octanol-1/PBS system.

To verify the absence of the ionic forms of chlorin e_6 in the octanol phase, we performed a qualitative assessment of its interphase distribution between octanol-1 and PBS/pH5.0, corresponding to the lower limit of the physiological range. Then, the absorption spectrum of the octanol phase belongs only to the electroneutral form $H_5Ce_6^{0/0}$ (Figure S7). The absence of the $H_6Ce_6^{+/0}$ cation (or its electroneutral associate with the counterion) in the nonpolar octanol phase, which is easily identified by characteristic optical spectra, makes it possible to exclude the presence of any other anionic form $H_2Ce_6^{0/3-}$, $H_3Ce_6^{0/2-}$ or $H_4Ce_6^{0/-}$ from the octanol phase.

A quantitative measure of the chlorin e_6 lipophilicity is the partial distribution coefficient (lipophilicity distribution coefficient) $H_5Ce_6^{0/0}$ between octanol-1 and an aqueous buffer solution ($\boldsymbol{p}_{Oct/PBS}$), the numerical value of which does not depend on the pH of the buffer solution (Equation (14))

$$p_{Oct/PBS} = \frac{\left[H_5Ce_6^{0/0}\right]_{Oct}}{\left[H_5Ce_6^{0/0}\right]_{PBS}} \quad (14)$$

Equation (14) assumes directly proportionality between the concentrations of electroneutral form $H_5Ce_6^{0/0}$ in the aqueous phase and in octanol-1. Traditionally, due to the uncertainty of the constants of protolytic Equilibria (9)-(13), the conditional partition coefficient ($\mathbf{P}_{Oct/PBS}$) is calculated for chlorin e_6 by Equation (15), which numerical value depends on the experimental pH.

$$P_{Oct/PBS} = \frac{\left[H_5Ce_6^{0/0}\right]_{Oct}}{C_0 - \left[H_5Ce_6^{0/0}\right]_{Oct}}, \quad (15)$$

where

$$C_0 - [H_5Ce_6^{0/0}]_{Oct} = ([H_2Ce_6^{0/3-}] + [H_3Ce_6^{0/2-}] + [H_4Ce_6^{0/-}] + [H_5Ce_6^{0/0}] + [H_7Ce_6^{+/0}])_{PBS} \ldots\ldots\ldots \quad (16)$$

Thus, it can be seen that unlike the constant $\boldsymbol{p}_{Oct/PBS}$, the value of $P_{Oct/PBS}$ is a conditional pH-dependent parameter equal to the ratio of the concentration of $H_5Ce_6^{0/0}$ in octanol to the total concentration of all equilibrium forms of chlorin e_6 in PBS at a fixed pH (Equation (16)). Published experimental values of $P_{Oct/PBS}$ for chlorin e_6 increase monotonically in the pH range of 7.1–7.6 and satisfactorily fit the straight line (black line in Figure 10).

On the other hand, the pH dependence of $[H_5Ce_6^{0/0}]_{PBS}$ concentration calculated from the K_{b1}, K_{b2}, K_{b3}^* and K_{b4} values, is extreme (Figure 9), which implies an extreme pH dependence for $[H_5Ce_6^{0/0}]_{Oct}$ (Equation (14)) and, as a consequence, for $P_{Oct/PBS}$ (Equation (15)). Thus, it should be assumed that in addition to $[H_5Ce_6^{0/0}]_{Oct}$, some other ionic forms of chlorin e_6 are involved in the proposed interphase equilibrium shown by Scheme 5. Using the method of fitting parameters of interfacial equilibrium it was found that this form is the $[H_6Ce_6^{+/0}]_{PBS}$ cation. Taking into account the sum of the current equilibrium concentrations of $[H_5Ce_6^{0/0}]_{PBS}$ (blue line, Figure 10) and $[H_6Ce_6^{+/0}]_{PBS}$ (green line, Figure 10) gives a sigmoid curve (Equation (17)), which tangent line is a linear pH dependence of experimental $P_{Oct/PBS}$ values (Figure 10), and the value of $p_{Oct/PBS}$ =13.77.

$$P_{Oct/PBS} = \frac{p_{Oct/PBS} \times \left(\left[H_5Ce_6^{0/0}\right] + \left[H_6Ce_6^{+/0}\right]\right)_{PBS}}{\left(\left[H_2Ce_6^{0/-3}\right] + \left[H_3Ce_6^{0/2-}\right] + \left[H_4Ce_6^{0/-}\right] + \left[H_5Ce_6^{0/0}\right] + \left[H_6Ce_6^{+/0}\right]\right)_{PBS}}, \quad (17)$$

where

$$p_{Oct/PBS}\left(\left[H_5Ce_6^{0/0}\right] + \left[H_6Ce_6^{+/0}\right]\right)_{PBS} = \left[H_5Ce_6^{0/0}\right]_{Oct} \quad (18)$$

In the extreme acidic region at pH < 3, where the sum (19) tends to zero, Equation (20) is valid

$$\left(\left[H_2Ce_6^{0/-3}\right] + \left[H_3Ce_6^{0/-2}\right] + \left[H_4Ce_6^{0/-}\right] + \left[H_5Ce_6^{0/0}\right]\right)_{PBS} \to 0 \quad (19)$$

$$P_{Oct/PBS} = p_{Oct/PBS} \text{ at } pH<3 \quad (20)$$

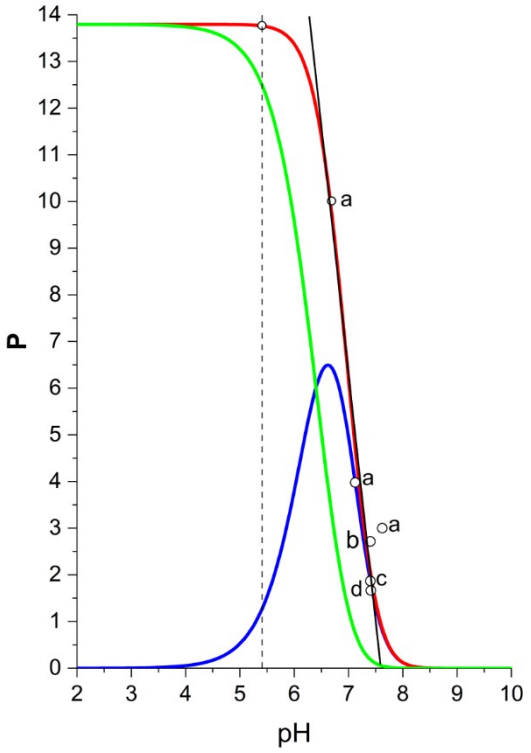

Figure 10. Theoretical pH dependences of $\mathbf{P}_{Oct/PBS}$ for $H_5Ce_6^{0/0}$ (blue line), for $H_6Ce_6^{+/0}$ (green line) and their sum (red line). The dots on the black line are experimental values $\mathbf{P}_{Oct/PBS}$/p*H* obtained for chlorin e_6 by different authors: a – 10/6.7, 4/7.1, 3/7.6;[16] b – 2.88/7.4;[52] c – 1.88/7.4;[50,51] d – 1.68/7.4.[10]

The obtained result indicates that the interface equilibrium (Scheme 4) "does not distinguish" between $H_5Ce_6^{0/0}$ and $H_5Ce_6^{+/0}$ in PBS. Obviously, the mechanism of chlorin e_6 interface equilibrium between octanol-1 and PBS requires further detailed investigation. The conclusion about the participation of the $H_6Ce_6^{+/0}$ cation in the chlorin e_6 interface equilibrium between octanol-1 and PBS allows us to highlight the key milestones of the chlorin e_6 interaction with the cancer tumor and its subsequent transport through the lipid membrane of a cancer cell consisting of lipophilic and hydrophilic layers:

1. Accumulation of $H_6Ce_6^{+/0}$ in the intercellular space, characterized by hyperacidity.
2. Increased adsorption of $H_6Ce_6^{+/0}$ on the cancer cells surface due to the high concentration of sialic acid and, as a result, a negative surface charge.
3. Effective transport of chlorin e_6 through the phospholipid membrane, consisting of lipophilic and hydrophilic layers, due to easy recharge between $H_5Ce_6^{0/0}$, which is able to accumulate in the lyophilic layer, and $H_6Ce_6^{+/0}$, which is able to accumulate in the lyophobic layer of phosphate groups.

Thus, protonation of chlorin platform is the most likely reason for the high selectivity of photosensitizer Fotoditazin® accumulation in tumor tissue.

Conclusions

Chlorin e_6 (H_2Ce_6) meets almost all the basic requirements for an optimal photosensitizer (PS) based on photophysical, biological and chemical – engineering criteria. The key feature of H_2Ce_6 is its inexhaustible natural raw material base. H_2Ce_6 is a unique molecular structure with p*H*-dependent charge and lipophilicity. It consists of a bulky alkyl-substituted chlorin platform and three close-packed residues of methanoic, ethanoic and propanoic acids at the molecule periphery. In aqueous solution, the H_2Ce_6 molecule undergoes stepwise p*H*-dependent acid-base ionization at three peripheral carboxyl groups and one intracyclic nitrogen atom of the chlorin platform, forming a series of amphiphilic ions: $H_2Ce_6^{0/-3}$, $H_2Ce_6^{0/-2}$, $H_2Ce_6^{0/-}$, $H_2Ce_6^{00}$, $H_2Ce_6^{+/0}$, characterized by close values of protolytic equilibrium constants. In the physiological and more acidic p*H* range corresponding to the microenvironment of cancer cells, there is an equilibrium mixture of five acid-base forms of chlorin e_6. As a result, the smart PS chlorin e_6 is able to adjust to a substrate of any polarity. The equilibrium of chlorin e_6 between octanol-1 and PBS involved $(H_2Ce_6^{00})_{Oct}$ and $(H_2Ce_6^{00} + H_2Ce_6^{+/0})_{PBS}$, as a result of easy recharge between $H_2Ce_6^{00}$ and $H_2Ce_6^{+/0}$ at the interface. This interfacial equilibrium monotonously shifts towards octalol-1 as the p*H* decreases, reaching the limiting value of distribution coefficient $P^*_{Oct/PBS}$=13.77. Protonation of the chlorin platform is likely the main reason for the high selectivity of the photosensitizer Fotoditazin® towards malignant neoplasms and its rapid diffusion across the lipid membrane of cancer cells.

Acknowledgements. This work was supported by RSF (Russian Science Foundation) according to the research project No. 23-23-00491. Equipment of the Shared Facility Center, the Upper Volga Regional Center of Physicochemical Studies was used.

References

1. Gilyadova A., Ishchenko A., Shiryaev A., Alekseeva P., Efendiev K., Karpova R., Loshchenov M., Loschenov V., Reshetov I. *Cancers (Basel)* **2022**, *14*(1), 211. https://doi.org/10.3390/cancers14010211
2. Hak A., Ali M.S., Sankaranarayanan S.A., Shinde V.R., Rengan A.K. *ACS Appl. Bio Mater*. **2023**, *6*, 349–364. https://doi.org/10.1021/acsabm.2c00891
3. Ni J., Yin X., Liao S., Cai M., Zhu R., Fu T., Du Y., Kong J., Zhang Y., Qu C., Dong X. *Mol. Pharmaceutics* **2023**, *20*, 875–885. https://doi.org/10.1021/acs.molpharmaceut.2c00824
4. da Vicente M.G.H., Smith K.M. *Molecules*. **2023**, *28*, 3479. https://doi.org/10.3390/molecules28083479.
5. Yu H., Huang Z., Wu J., Zhao Z., Hua Y., Yang Y. *Nanomedicine* **2025**, *20*, 389–400. https://doi.org/10.1080/17435889.2025.2456450.
6. Kustov A.V. *ChemChemTech* **2023**, *66*(12), 32–40. https://doi.org/10.6060/ivkkt.20236612.6902.
7. Berezin D.B., Bondareva T.V., Shukhto O.V., Kustova T.V., Razgovorov P.B., Kustov A.V. *ChemChemTech* **2025**, *68*(6), 70–82. https://doi.org/10.6060/ivkkt.20256806.7166.
8. Parkhats M.V., Galievskii V.A., Zharnikova E.S., Knyukshto V.N., Lepeshkevich S.V., Stashevskii A.S., Trukhacheva T.V., Dzhagarov B.M. *J. Appl. Spectrosc.* **2011**, *78*, 278–285. https://doi.org/10.1007/s10812-011-9459-0.

9. do Amaral S.R., Aires-Fernandes M., Haddad F.F., Gini A.L.R., Scarim C.B., Primo F.L. *Molecules* **2025**, *30*(3), 544. https://doi.org/10.3390/molecules30030544.
10. Isakau H.A., Parkhats M.V., Knyukshto V.N., Dzhagarov B.M., Petrov E.P., Petrov P.T. *J. Photochem. Photobiol. B Biol.* **2008**, *92*(3), 165–174. https://doi.org/10.1016/j.jphotobiol.2008.06.004.
11. Losytskyy M.Y., Kharchenko R.A., Harahuts Y.I., Virych P.A., Kutsevol N.V., Yashchuk V.M. *Funct. Mater.* **2020**, *27*, 12–17. https://doi.org/10.15407/fm27.01.12.
12. Fernandez J.M., Bilgin M.D., Grossweiner L.I. *J. Photochem. Photobiol. B Biol.* **1997**, *37*, 131–140. https://doi.org/10.1016/S1011-1344(96)07349-6.
13. Parkhats M.V., Galievsky V.A., Stashevsky A.S., Trukhacheva T.V., Dzhagarov B.M. *Opt. Spectrosc.* **2009**, *107*, 974–980. https://doi.org/10.1134/S0030400X09120200.
14. *Concentrate for preparation of infusions solution*. https://fotoditazin.com/produktsiya/?ELEMENT_ID=24 (accessed 2025-08-01).
15. *Global Spirulina Market - 2025-2032*. https://www.market-research.com/DataM-Intelligence-4Market-Research-LLP-v4207/Global-Spirulina-41227043/ (accessed 2025-08-01).
16. Čunderlíková B., Gangeskar L., Moan J. *J. Photochem. Photobiol. B Biol.* **1999**, *53*, 81–90. https://doi.org/10.1016/S1011-1344(99)00130-X.
17. Čunderlíková B., Kongshaug M., Gangeskar L., Moan J. *Int. J. Biochem. Cell Biol.* **2000**, *32*, 759–768. https://doi.org/10.1016/S1357-2725(00)00015-7.
18. Mojzisova H., Bonneau S., Vever-Bizet C., Brault D. *Biochim. Biophys. Acta - Biomembr.* **2007**, *1768*, 366–374. https://doi.org/10.1016/j.bbamem.2006.10.009.
19. Mojzisova H., Bonneau S., Vever-Bizet C., Brault D. *Biochim. Biophys. Acta - Biomembr.* **2007**, *1768*, 2748–2756. https://doi.org/10.1016/j.bbamem.2007.07.002.
20. Zorin V.P., Michalovsky I., Zorina T.E., Khludeyev I.I. *Proc. SPIE 2625, Photochemotherapy: Photodynamic Therapy and Other Modalities* **1996**, *2625*, 146–155. https://doi.org/10.1117/12.230981.
21. Gullino P.M., Grantham F.H., Smith S.H., Haggerty A.C. *J. Natl. Cancer Inst.* **1965**, *34*, 857–869. https://doi.org/10.1093/jnci/34.6.857.
22. Thistlethwaite A.J., Leeper D.B., Moylan D.J., Nerlinger R.E. *Int. J. Radiat. Oncol.* **1985**, *11*, 1647–1652. https://doi.org/10.1016/0360-3016(85)90217-2.
23. Wike-Hooley J.L., Haveman J., Reinhold H.S. *Radiother. Oncol.* **1984**, *2*, 343–366. https://doi.org/10.1016/S0167-8140(84)80077-8.
24. Kuzelova K., Brault D. *Biochemistry* **1995**, *34*, 11245–11255. https://doi.org/10.1021/BI00035A034.
25. Moan J., Smedshammer L., Christensen T. *Cancer Lett.* **1980**, *9*, 327–332. https://doi.org/10.1016/0304-3835(80)90025-7.
26. Thomas J.P., Girotti A.W. *Photochem. Photobiol.* **1989**, *49*, 241–247. https://doi.org/10.1111/J.1751-1097.1989.TB04102.X
27. Falk J.E. In: *Porphyrins and Metalloporphyrins* (Smith K.M., Ed.), Elsevier Science Ltd, **1975**.
28. Zharov E., Zharov I., Loginov F. *Method of Producing Tris-sodium Salt of Chlorin e_6,* **2019**. https://patents.google.com/patent/RU2705199C1/en (accessed 2025-08-02).
29. Frisch M.J., Trucks G.W., Schlegel H.B., Scuseria G.E., Robb M.A., *et al. Gaussian 09.* Gaussian, Inc., Wallingford CT, **2009**.
30. Sheinin V.B., Ivanova Y.B. *Russ. J. Phys. Chem. A* **2007**, *81*, 1250–1255. https://doi.org/10.1134/S0036024407080134
31. Sheinin V. B., Ivanova Y. B. *Russ. J. Inorg. Chem.* **2005**, *50*, 1098–1107.
32. Sheinin V.B., Kulikova O.M., Koifman O.I. *Macroheterocycles* **2018**, *11*, 363–370. https://doi.org/10.6060/mhc181109S.
33. Sheinin V.B., Kulikova O.M., Koifman O.I. *J. Mol. Liq.* **2019**, *277*, 397–408. https://doi.org/10.1016/j.molliq.2018.12.105.
34. Sheinin V.B., Ratkova E.L., Mamardashvili N.Z. *J. Porphyrins Phthalocyanines* **2008**, *12*, 1211–1219. https://doi.org/10.1142/S1088424608000595.
35. Sheinin V.B., Simonova O.R., Ratkova E.L. *Macroheterocycles* **2008**, *1*, 72–78. https://doi.org/ 10.6060/mhc2008.1.72
36. Sheinin V.B., Kulikova O.M. *Dyes Pigm.* **2021**, *194*, 109589. https://doi.org/10.1016/j.dyepig.2021.109 589.
37. Sheinin V.B., Ivanov D.A., Koifman O.I. *Macroheterocycles* **2017**, *10*, 487–495. https://doi.org/ 10.6060/mhc170833s.
38. Sheinin V.B., Bobritskaya E.V., Shabunin S.A., Koifman O.I. *Macroheterocycles* **2014**, *7*, 209–217. https://doi.org/10.6060/mhc141033s.
39. Sheinin V.B., Shabunin S.A., Bobritskaya E.V., Ageeva T.A., Koifman O.I. *Macroheterocycles* **2012**, *5*, 252–259. https://doi.org/10.6060/MHC2012.120989S.
40. Sheinin V.B., Shabunin S.A., Bobritskaya E.V., Koifmana O.I. *Macroheterocycles* **2011**, *4*, 80–84. https://doi.org/10.6060/mhc2011.2.02.
41. Sheinin V.B., Ivanova Y.B., Berezin B.D. *Russ. J. Gen. Chem.* **2002**, *72*, 1128–1131. https://doi.org/10.1023/A:1020719303646/METRICS.
42. Izutsu K. *Electrochemistry in Nonaqueous Solutions,* Wiley-VCH Verlag GmbH & Co. KGaA, **2002**. https://doi.org/10.1002/3527600655.
43. Vermathen M., Marzorati M., Vermathen P., Bigler P. *Langmuir* **2010**, *26*, 11085–11094. https://doi.org/10.1021/la100679y.
44. Hynninen P.H. *J. Porphyrins Phthalocyanines* **2014**, *18*, 385–395. https://doi.org/10.1142/S1088424614500126.
45. Hynninen P.H. *J. Porphyrins Phthalocyanines* **2012**, *16*, 1167–1176. https://doi.org/10.1142/S1088424612501167.
46. Hynninen P.H. *J. Chem. Soc. Perkin Trans. 2* **1991**, *2*, 669–678. https://doi.org/10.1039/p29910000669.
47. Brault D., Vever-Bizet C., Le Doan T. *Biochim. Biophys. Acta - Biomembr.* **1986**, *857*, 238–250. https://doi.org/10.1016/0005-2736(86)90352-4.
48. Saini R.K., Dube A., Gupta P.K., Das K. *J. Phys. Chem. B* **2012**, *116*, 4199–4205. https://doi.org/10.1021/JP205 335Z.
49. Khludeev I.I., Kozyr' L.A., Zorina T.E., Zorin V.P. *Bull. Exp. Biol. Med.* **2015**, *160*, 208–212. https://doi.org/10.1007/S10517-015-3130-3.
50. Kustov A.V., Berezin D.B., Zorin V.P., Morshnev P.K., Kukushkina N.V., *et al. Pharmaceutics* **2023**, *15*, 61. https://doi.org/10.3390/pharmaceutics15010061.
51. Kustov A.V., Morshnev P.K., Kukushkina N.V., Smirnova N.L., Berezin D.B., *et al. Int. J. Mol. Sci.* **2022**, *23*, 5294. https://doi.org/ 10.3390/ijms23105294.
52. Douillard S., Lhommeau I., Olivier D., Patrice T. *J. Photochem. Photobiol. B Biol.* **2010**, *98*, 128–137. https://doi.org/10.1016/j.jphotobiol.2009.11.011.
53. Scolaro L.M., Castriciano M., Romeo A., Patanè S., Cefalì E., Allegrini M. *J. Phys. Chem. B* **2002**, *106*, 2453–2459. https://doi.org/10.1021/jp013155h.
54. Martin R.B. *Science* **1963**, *139*, 1198–1203. https://doi.org/10.1126/science.139.3560.1198.
55. Donder T., Van Rysselberghe P. *Thermodynamic Theory of Affinity: A Book of Principles,* Stanford University Press, **1936**.

Received 24.09.2025
Accepted 14.10.2025